*lubricants*

MDPI

*Article*

# Effect of Bio-Based, Mixed Ester Lubricant in Minimum Quantity Lubrication on Tool Wear and Surface Integrity in Ultra-Precision Fly-Cutting of KDP Crystals

**Xuelian Yao [1,2,*], Feihu Zhang [1], Shuai Zhang [2], Jianfeng Zhang [2], Defeng Liao [2], Xiangyang Lei [2], Jian Wang [2] and Jianbiao Du [1]**

[1] School of Mechatronics Engineering, Harbin Institute of Technology, Harbin 150001, China
[2] Laser Fusion Research Center, China Academy of Engineering Physics, Mianyang 621900, China
* Correspondence: xlyao93@163.com

**Abstract:** Potassium dihydrogen phosphate (KDP) crystals, vital for high-power laser systems, pose significant machining challenges due to their brittleness, low hardness, and hygroscopic properties. Achieving crack-free, high-precision surfaces is essential but complex. Single-point diamond fly-cutting (SPDF) is the primary method, yet it exposes tools to high mechanical stress and heat, accelerating wear. In dry cutting, worn tools develop adhesive layers that detach, causing scratches and degrading surface quality. Traditional wet cutting improves surface finish but leaves residual fluids that contaminate the surface with metal ions, leading to optical degradation and fogging. To address these issues, this study explores mixed-fat-based minimum quantity lubrication (MQL) as a sustainable alternative, comparing two lubricants: biodegradable-base mixed ester lubrication (BBMEL) and hydrocarbon-based synthetic lubricant (HCBSL). A comprehensive evaluation method was developed to analyze surface roughness, tool wear, and subsurface damage under dry cutting, MQL-BBMEL, and MQL-HCBSL conditions. Experimental results show that MQL-BBMEL significantly enhances machining performance, reducing average surface roughness by 27.77% (*Sa*) and 44.77% (*Sq*) and decreasing tool wear by 25.16% compared to dry cutting, outperforming MQL-HCBSL. This improvement is attributed to BBMEL's lower viscosity and higher proportion of polar functional groups, which form stable lubricating films, minimizing friction and thermal effects. Structural analyses confirm that MQL-BBMEL prevents KDP crystal deliquescence and surface fogging. These findings establish MQL-BBMEL as an eco-friendly, high-performance solution for machining brittle optical materials, offering significant advancements in precision machining for high-power laser systems.

**Keywords:** bio-based lubricant; MQL; ultra-precision fly-cutting; KDP crystals; surface integrity; tool wear

check for updates

Received: 28 February 2025
Revised: 21 March 2025
Accepted: 26 March 2025
Published: 1 April 2025

**Citation:** Yao, X.; Zhang, F.; Zhang, S.; Zhang, J.; Liao, D.; Lei, X.; Wang, J.; Du, J. Effect of Bio-Based, Mixed Ester Lubricant in Minimum Quantity Lubrication on Tool Wear and Surface Integrity in Ultra-Precision Fly-Cutting of KDP Crystals. *Lubricants* **2025**, *13*, 156. https://doi.org/10.3390/lubricants13040156

**Copyright:** © 2025 by the authors. Licensee MDPI, Basel, Switzerland. This article is an open access article distributed under the terms and conditions of the Creative Commons Attribution (CC BY) license (https://creativecommons.org/licenses/by/4.0/).

## 1. Introduction

Potassium dihydrogen phosphate (KDP) crystals, known for their exceptional nonlinear optical properties and high transmittance, are indispensable in high-power laser systems and inertial confinement fusion applications [1,2]. These applications demand unparalleled optical uniformity and surface quality. However, the soft-brittle nature of KDP crystals, coupled with their sensitivity to stress, temperature fluctuations, and susceptibility to hydrolysis, poses significant machining challenges. Traditional grinding and polishing methods often embed abrasive particles into the surface, reducing the laser

damage threshold and failing to meet practical requirements [3–5]. Single-point diamond fly-cutting (SPDF) has emerged as the preferred technique for processing large-aperture KDP crystals due to its ability to minimize anisotropic effects and improve surface quality [6–8]. However, the transient cutting characteristics of SPDF subject tools to considerable mechanical stress and thermal loads, accelerating wear on the cutting edges. Under dry cutting conditions, friction and adhesion intensify as oxygen-containing functional groups on the worn tool surface chemically bond with chips, forming adhesive layers. These layers repeatedly form and detach, resulting in surface scratches [9]. Consequently, lubrication technology has become essential for extending tool life, enhancing machining performance, and reducing surface defects.

Extensive studies have demonstrated that lubrication conditions play a critical role in interfacial wear mechanisms. Effective lubrication not only reduces frictional forces but also enhances surface quality between contact surfaces [10–13]. While mineral oil-based lubrication in wet cutting can improve the surface quality of KDP crystals to some extent, it has significant drawbacks. Residual cutting fluids often cause haze on the crystal surface, reducing laser transmittance by about 20% [14]. Furthermore, contaminants like Al, Zn, and Na ions from the oil can adsorb onto the crystal, further degrading its optical properties [15]. The environmental and health risks associated with mineral oil-based lubricants also conflict with the principles of sustainable manufacturing [16]. More critically, excessive oil penetration during wet cutting can increase adhesion between the KDP crystal and the vacuum chuck, making it difficult to remove the workpiece even after deactivating the vacuum system. Additionally, mineral oil lubricants tend to form stubborn oil films on the crystal surface, complicating the cleaning process. Given these challenges, mineral oil-based wet cutting is unsuitable for the precision machining of large-diameter KDP crystals.

To address these issues, researchers have increasingly turned to greener and more efficient lubrication methods. Minimal quantity lubrication (MQL) has emerged as a promising alternative, offering low lubricant consumption, effective lubrication, and reduced environmental impact [17–19]. MQL operates by atomizing lubricants into micron-sized droplets via high-pressure air, delivering them precisely to the cutting zone [20–22]. This approach effectively reduces friction and cutting heat, enhancing surface quality while minimizing pollution and resource waste [23]. Zhou et al. [24] evaluated three vegetable-based cutting fluids in an MQL system, revealing that rapeseed oil outperformed others by reducing cutting forces, temperatures, and tool wear compared to dry cutting. Su et al. [25] demonstrated that nanofluid-based MQL significantly lowered cutting forces and temperature in the machining of AISI 1045 carbon steel, highlighting its potential for precision applications. Additionally, Li et al. [26] reported that MQL increased the durability of TiAlN-coated tools by 49% and reduced adhesive wear in milling magnesium-rare earth alloys. Although MQL (minimum quantity lubrication) technology has made significant progress in metal processing, the selection of lubricants remains a key challenge. Traditional vegetable oils are widely recognized for their biodegradability and environmental friendliness [27,28], but their poor oxidation stability and limited high-pressure performance restrict their practical applications [29–31]. While chemical modification techniques, such as epoxidation and nanoparticle additives, can enhance their properties, these methods may trigger adverse chemical reactions with KDP crystal surfaces, increasing cleaning difficulties. Additionally, the high viscosity of vegetable oils reduces their penetration efficiency at the tool–workpiece interface, negatively affecting lubrication during processing [32].

In contrast, bio-based lubricants demonstrate superior oxidation stability and high-pressure performance, making them more effective in MQL applications. Their enhanced chemical stability and high-pressure lubrication significantly improve processing efficiency

and surface quality. Debnath, S. et al. [33] demonstrated that bio-based, mixed ester lubricants enhance machinability by improving heat dissipation and reducing tool wear in MQL systems compared to conventional vegetable oils. Lisowicz, J. et al. [34] reported that a 50% vegetable oil + 50% diester mixture significantly improved surface finish and reduced cutting forces in Ti-6Al-4V machining under MQL conditions. Farfan-Cabrera, L.I. et al. [35] highlighted the potential of microalgae oils as sustainable bio-based lubricants for MQL, offering superior performance and eco-friendliness compared to conventional fluids. Panda, D. et al. [36] found that bio-based, mixed ester lubricants with nanoparticles reduce tool wear, cutting forces, and power consumption while improving surface finish in MQL machining.

However, traditional bio-oil cutting fluids still face notable issues in practical use. High-viscosity fluids, despite their higher flash points, exhibit poor fluidity and are difficult to atomize effectively. Low-viscosity fluids, while easier to atomize, have lower flash points, posing safety risks. This is particularly critical in fly cutting, where the sudden impact and energy release during tool engagement may lead to safety hazards if the cutting fluid's flash point is too low. Therefore, selecting cutting fluids with moderate viscosity and higher flash points is essential. Finding biodegradable synthetic esters that meet multiple performance criteria remains a pressing technological challenge. These materials must not only provide excellent tool protection and wear resistance but also prevent the formation of adhesion layers during processing and be compatible with toluene-based cleaning systems. Moreover, they must ensure no deliquescence or fogging occurs on KDP crystal surfaces. These stringent requirements significantly raise the technical barriers and application difficulties in material development.

This study explores a sustainable lubrication strategy for MQL applications, utilizing highly biodegradable, mixed-fat-based lubricants. By comparing dry cutting with MQL using two types of mixed-fat, oil-based lubricants, this research evaluates their effectiveness in reducing tool wear, enhancing surface quality, and minimizing environmental impact. The investigation focuses on assessing machining performance under different cutting conditions and distances, with particular emphasis on surface integrity and lubrication mechanisms. This study addresses a critical gap in the application of bio-lubricants in the ultra-precision machining of brittle materials, contributing to the advancement of green manufacturing technologies.

## 2. Experimental Setup

### *2.1. Experimental Setup and Materials*

The experiments were conducted using an ultra-precision, single-point diamond fly-cutting machine to investigate the effects of bio-lubricant-based minimal quantity lubrication (MQL) on surface quality and friction characteristics. In the OXYZ coordinate system shown in Figure 1, the nozzle's spatial position was determined through the following steps: First, a KDP crystal fixed on the platform served as the reference, with one of its edges as the origin. The nozzle was then positioned in the coordinate system and defined as the initial point. Subsequently, the nozzle was elevated to a height $h$ above the reference plane and set at a horizontal distance $w$ from the reference edge. Finally, the nozzle axis was oriented at a 45° angle to the OX axis to ensure precise alignment with the cutting zone. This configuration facilitated efficient lubrication and cooling in the cutting area. The experimental setup is illustrated in Figure 1.

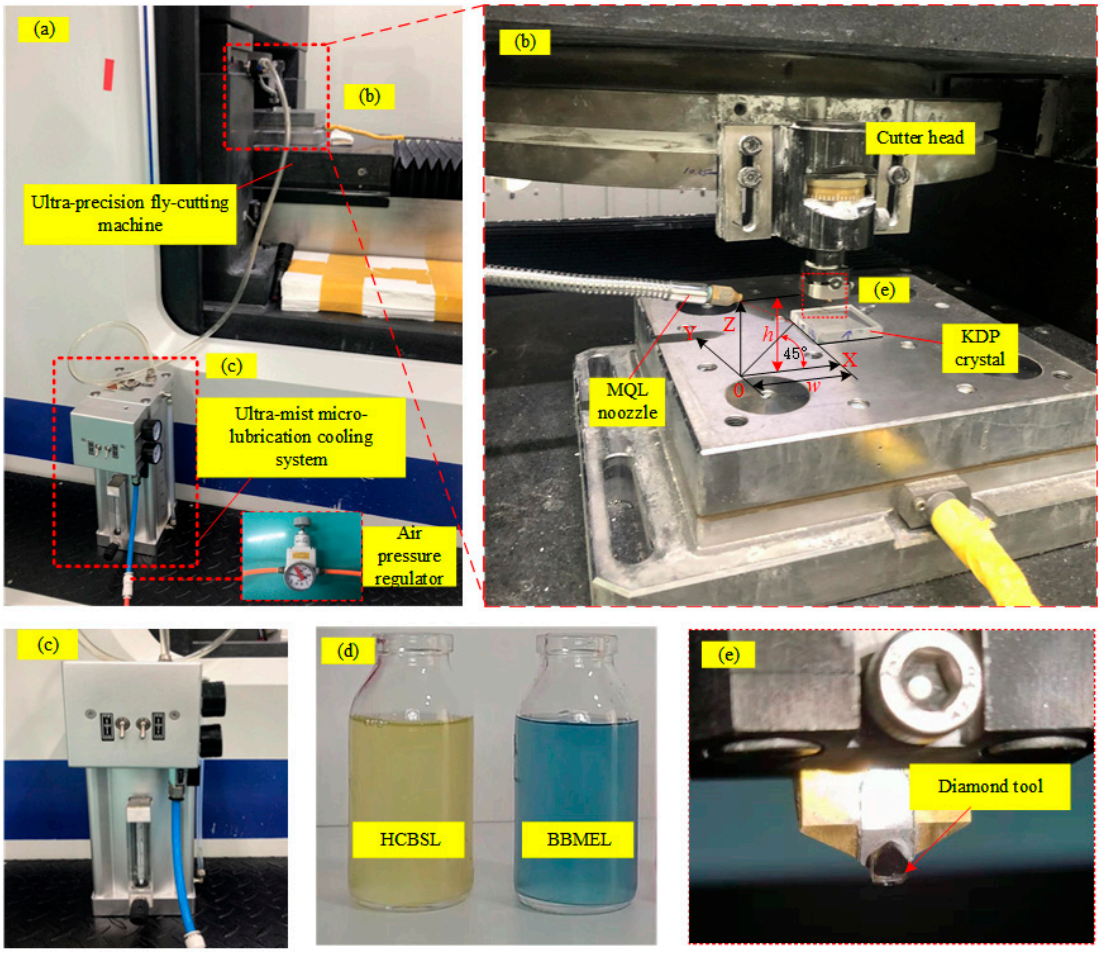



**Figure 1.** Experimental setup of the ultra-mist micro-lubrication system for assisting in fly-cutting KDP crystals: (**a**) ultra-precision fly-cutting machine; (**b**) setup of the KDP crystal, cutting tool, and MQL nozzle; (**c**) ultra-mist micro-lubrication cooling system; (**d**) lubricant; (**e**) diamond cutting tool.

The experimental material used in this study was a type II KDP crystal with dimensions of 50 mm × 50 mm × 10 mm. To ensure consistency across experiments, the surface of the crystal underwent precision fly-cutting, achieving a surface roughness of Ra < 2 nm. Natural diamond tools were utilized, featuring a rake angle of 45°, a clearance angle of 25°, and a tool tip radius of 5 mm. To investigate tool wear and tool cutting edge morphology under different lubrication conditions, the discrete cutting distance method was employed. In this approach, a separate tool from the same batch was assigned to each cutting distance, enabling an indirect analysis of tool wear. This method effectively eliminates potential errors caused by repeated disassembly and reinstallation of the same tool. The experimental plan is outlined in Table 1.

**Table 1.** Comparison of experimental configurations for diamond tool in SPDF.

| Group | Cutting Method | Tool Numbers | Cutting Distances (km) |
|---|---|---|---|
| 1–4 | Dry | D1–D4 | 20, 40, 60, 80 |
| 5–8 | MQL-BBMEL | B1–B4 | 20, 40, 60, 80 |
| 9–12 | MQL-HCBSL | H1–H4 | 20, 40, 60, 80 |

### *2.2. Lubricants and Experimental Conditions*

The experiment was conducted using two lubricants: a bio-based, mixed ester lubricant (BBMEL) and a hydrocarbon-based synthetic lubricant (HCBSL), both formulated from

mixed fats. Their key compositions and properties are summarized in Table 2. To evaluate lubrication performance, three cutting conditions were tested: dry cutting, the MQL system with BBMEL (MQL-BBMEL), and the MQL system with HCBSL (MQL-HCBSL). The objective was to compare the effectiveness of each lubricant in enhancing surface quality and reducing tool wear during ultra-precision fly-cutting. A controlled variable methodology was employed, ensuring that only the type of lubricant varied, while all other experimental parameters remained constant. This approach allowed for a direct assessment of lubricant influence on cutting performance and surface integrity. The cutting parameters used in the experiment are summarized in Table 3.

**Table 2.** Composition and properties of lubricants.

| Properties of Lubricants | Base Composition | Chemical Formula | Kinematic Viscosity ($mm^2/s$) | Water Content (ppm) | Flash Point (°C) |
|---|---|---|---|---|---|
| BBMEL | BBMEL: 93.25% Dioctyl Adipate, 3.24% Ethylene Glycol Laurate, 1.51% Castor Oil Ethoxylate, 2.00% Others | Dioctyl Adipate ($C_{22}H_{42}O_4$), Ethylene Glycol Laurate ($C_{14}H_{28}O_3$), Castor Oil Ethoxylate ($C_{57}H_{104}O_9 + nC_2H_4O$, n varies) | 16 | 456 | 220 |
| HCBSL | HCBSL: 90.85% Hydrocarbon-based synthetic oily mixture, 3.74% Trimethylpentene, 2.82% Partially ethoxylated trimethylene derivative, 2.59% Others | Hydrocarbon-based synthetic oily mixture ($C_{24}H_{50}$), Trimethylpentene ($C_8H_{16}$), Partially ethoxylated trimethylene derivative ($C_3H_6(OCH_2CH_3)$ OH) | 48 | 584 | 320 |

**Table 3.** Cutting parameters and lubrication details.

| | |
|---|---|
| Cutting speed (m/s) | 15 |
| Feed rate (μm/r) | 50 |
| Cutting depth (μm) | 5 |
| Cutting environment | Dry, MQL |
| Air pressure (μm) | 0.3 |
| Flow rate (mL/h) | 30 |
| Droplet size (μm) | 5 |
| Nozzle–workpiece edge distance (mm) | 110 |
| Nozzle height *h* (mm) | 58 |
| Nozzle horizontal distance *w* (mm) | 78 |
| Nozzle angle in X–Y plane | 45° |

### *2.3. Experimental Characterization*

After cutting, surface morphology and roughness were evaluated using an optical profiler (Zygo New View 8200, Zygo Corporation, Middlefield, CT, USA) and a confocal microscope to observe the optical appearance of the KDP crystal surface. Following each cutting session, the tool was removed, and changes in the cutting edge radius were examined using an atomic force microscope (AFM, Oxford Instruments, Abingdon, UK). To investigate the adhesion layer formed on the tool surface under both dry cutting and MQL conditions, scanning electron microscopy (SEM, Thermo Scientific K-Alpha, Thermo Fisher Scientific, Waltham, MA, USA) was employed. Energy-dispersive spectroscopy (EDS) was used in conjunction with SEM to analyze the composition and distribution of the adhesion layer. Additionally, the chemical composition of the optimal lubricant was

examined using Fourier transform infrared spectroscopy (FTIR, Thermo Scientific Nicolet iS50, Thermo Fisher Scientific, Waltham, MA, USA) and X-ray photoelectron spectroscopy (XPS, Thermo Scientific K-Alpha, Thermo Fisher Scientific, Waltham, MA, USA), focusing on the chemical interactions between the lubricant and the tool surface. Following each experiment, the tools were ultrasonically cleaned for 30 min using a Bakr BK-80D ultrasonic cleaner (Bakr Ultrasonic, Shenzhen, China). Post-cleaning XPS analysis was performed to verify any changes in surface composition and assess the durability of the lubrication effects. To further explore the impact of lubrication on the surface integrity of the KDP crystals, grazing incidence X-ray diffraction (GIXRD, Rigaku Smartlab 3 kW, Rigaku Corporation, Tokyo, Japan) and Raman spectroscopy (Horiba LabRAM HR Evolution, Horiba Ltd., Kyoto, Japan) were utilized to analyze the subsurface lattice and surface characteristics of the KDP crystals. This analysis provided insights into how the mixed-fat lubricant influenced the surface integrity of the crystals.

## 3. Results and Discussion

### *3.1. Surface Quality and Morphological Characteristics*

#### 3.1.1. Surface Roughness Analysis Under Different Cutting Conditions

Surface roughness is a critical indicator of machining quality, and its evaluation relies on fundamental metrology parameters. The arithmetic average roughness (*Sa*) represents the arithmetic mean of the absolute deviations of the surface height from the mean plane. Mathematically, it is expressed as the following:

$$Sa = \frac{1}{A}\iint_A |Z(x,y) - \overline{Z}|dxdy \tag{1}$$

where $A$ denotes the total area of the measured region, $Z(x,y)$ is the height of the surface at the point $(x,y)$, and $Z^-$ is the mean height of the surface, calculated as

$$\overline{Z} = \frac{1}{A}\iint_A Z(x,y)dxdy \tag{2}$$

Another critical parameter in surface analysis is the root mean square roughness (*Sq*), which quantifies the root mean square of the deviations of the surface height from the mean plane. It is defined as the following:

$$Sq = \sqrt{\frac{1}{A}\iint_A (Z(x,y) - \overline{Z})^2 dxdy} \tag{3}$$

Figures 2 and 3 illustrate the surface roughness variations at different cutting distances under various lubrication conditions. Compared to dry cutting, MQL-BBMEL achieved significant improvements in surface quality, reducing both *Sa* and *Sq* across all cutting distances. At 20 km, 40 km, 60 km, and 80 km, MQL-BBMEL reduced *Sa* by 17.67%, 24.74%, 38.05%, and 30.62%, respectively, averaging a 27.77% reduction. For *Sq*, MQL-BBMEL achieved reductions of 14.67%, 47.39%, 62.70%, and 54.29%, averaging 44.76%. In contrast, MQL-HCBSL showed more modest improvements, reducing *Sa* by 0.99%, 19.09%, 23.75%, and 23.95%, averaging 16.94%, and *Sq* by 0.59%, 29.98%, 42.14%, and 37.48%, averaging 27.55%. The difference in performance between the two lubricants increased with longer cutting distances, with MQL-BBMEL consistently maintaining lower roughness values at all intervals. For instance, at 80 km, MQL-BBMEL achieved reductions of 30.62% in *Sa* and 54.29% in *Sq*, whereas MQL-HCBSL yielded comparatively lower reductions of 23.95% in *Sa* and 37.48% in *Sq*. These results indicate that MQL-BBMEL achieved significantly better

surface roughness reduction than MQL-HCBSL, particularly at longer cutting distances. The trend suggests that MQL-BBMEL maintains more effective lubrication, reducing surface defects more efficiently over time. The observed variations in roughness values between the two MQL conditions will be further discussed in subsequent sections.

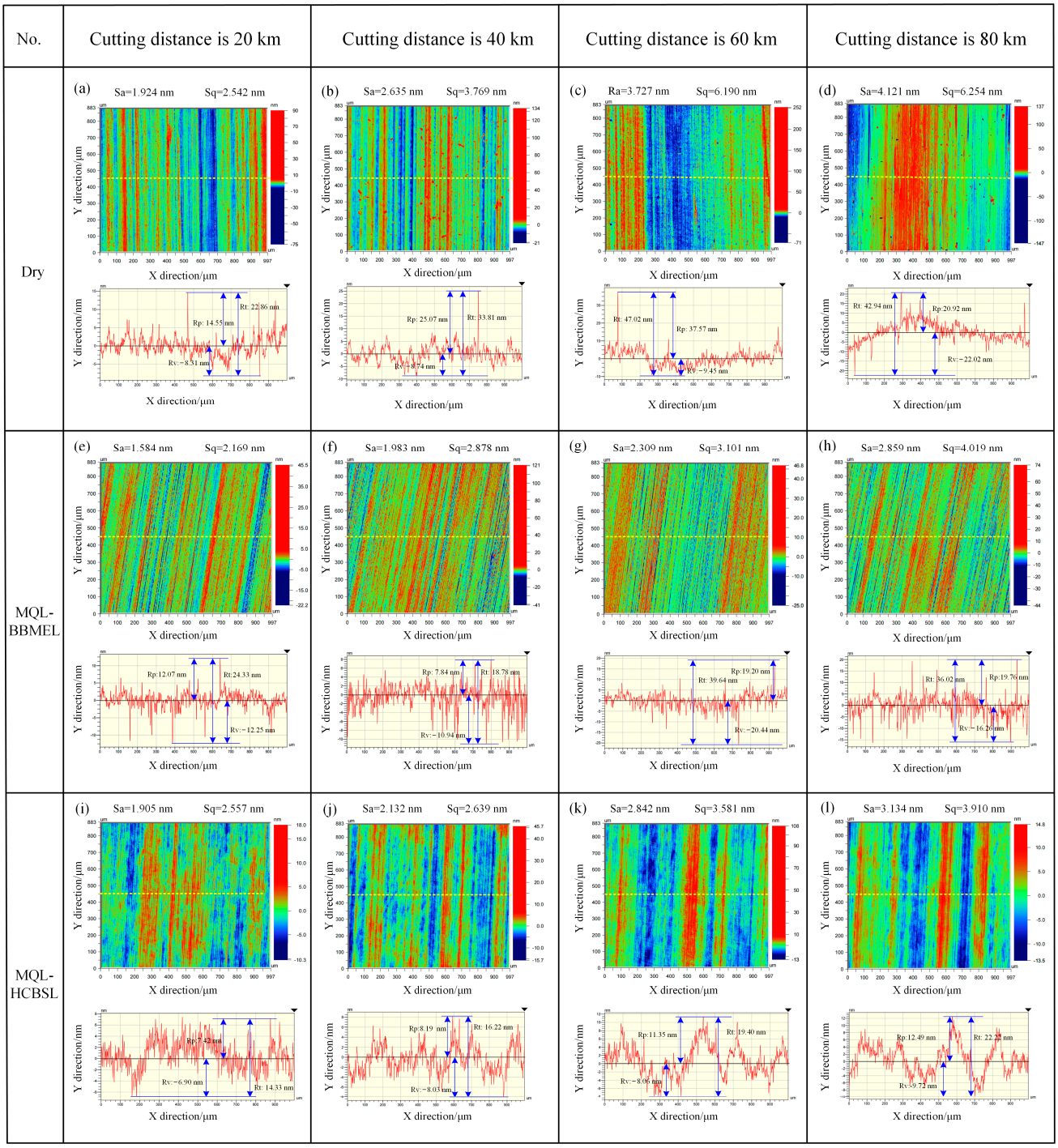



**Figure 2.** Surface roughness under dry cutting and MQL conditions after a cutting distance of 20 km, 40 km, 60 km, and 80 km. (**a**–**d**) Dry cutting; (**e**–**h**) MQL-BBMEL; (**i**–**l**) MQL-HCBSL.

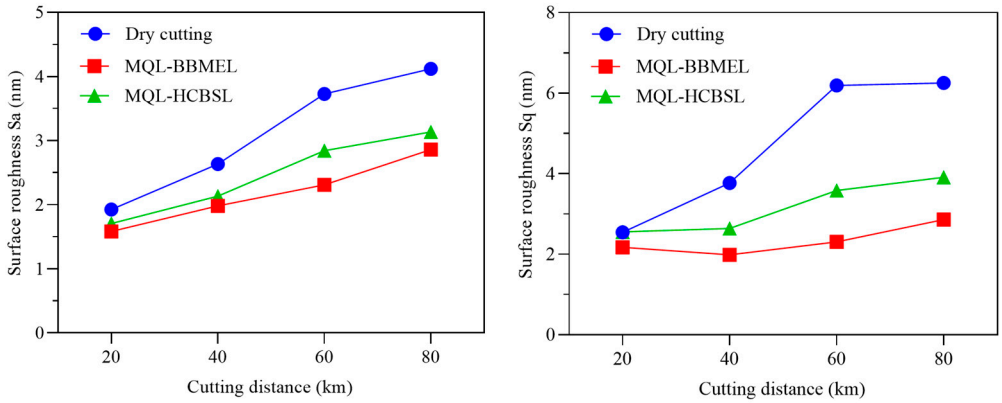



**Figure 3.** The variation of *Sa* and *Sq* under dry cutting and MQL conditions at different cutting distances. (**a**) *Sa*; (**b**) *Sq*.

To further investigate and evaluate the surface characteristics, the critical surface roughness parameters root-mean-square roughness (*Rq*), total height of roughness profile (*Rt*), maximum profile peak height (*Rp*), and maximum profile valley depth (*Rv*) were analyzed based on the methodology adopted in references [37–39]. These parameters provide a comprehensive representation of the surface morphology, and their corresponding formulas are as follows:

$$Rq = \sqrt{\frac{1}{n}\sum_{i=1}^{n} z_i^2} \tag{4}$$

where $z_i$ represents the height of the surface profile at the $i$-th point and $n$ is the total number of measured points.

$$Rt = Rp + Rv \tag{5}$$

where *Rp* is the maximum peak height and *Rv* is the maximum valley depth.

$$R_p = \max(z_i) \tag{6}$$

$$R_v = |\min(z_i)| \tag{7}$$

The surface roughness parameters *Rq*, *Rt*, *Rp*, and *Rv* were evaluated across various cutting distances under dry cutting and MQL conditions, as illustrated in Figure 4. Dry cutting consistently produced the highest roughness values, with *Rq* increasing from 2.49 nm at 20 km to 4.80 nm at 80 km and *Rt* reaching its peak of 47.02 nm at 60 km. In contrast, both MQL-BBMEL and MQL-HCBSL significantly reduced surface roughness, with MQL-HCBSL demonstrating superior performance. Specifically, Rt values under MQL-HCBSL ranged from 14.33 nm at 20 km to 22.22 nm at 80 km, consistently lower than those observed under dry cutting and MQL-BBMEL. A detailed analysis of *Rp* and *Rv* further underscores the differences between these conditions. Under dry cutting, *Rp* exhibited considerable variability, increasing from 14.55 nm at 20 km to a peak of 37.57 nm at 60 km before declining to 20.92 nm at 80 km. Conversely, MQL-BBMEL maintained more stable *Rp* values, ranging from 7.84 nm to 19.76 nm, while MQL-HCBSL consistently produced the lowest *Rp* values, improving from 7.42 nm at 20 km to 12.49 nm at 80 km. Similarly, *Rv* under dry cutting increased sharply from 8.31 nm at 20 km to 22.02 nm at 80 km. In comparison, both MQL-BBMEL and MQL-HCBSL effectively controlled *Rv*, with MQL-HCBSL achieving the most stable and lowest values, remaining below 9.73 nm across all cutting distances.

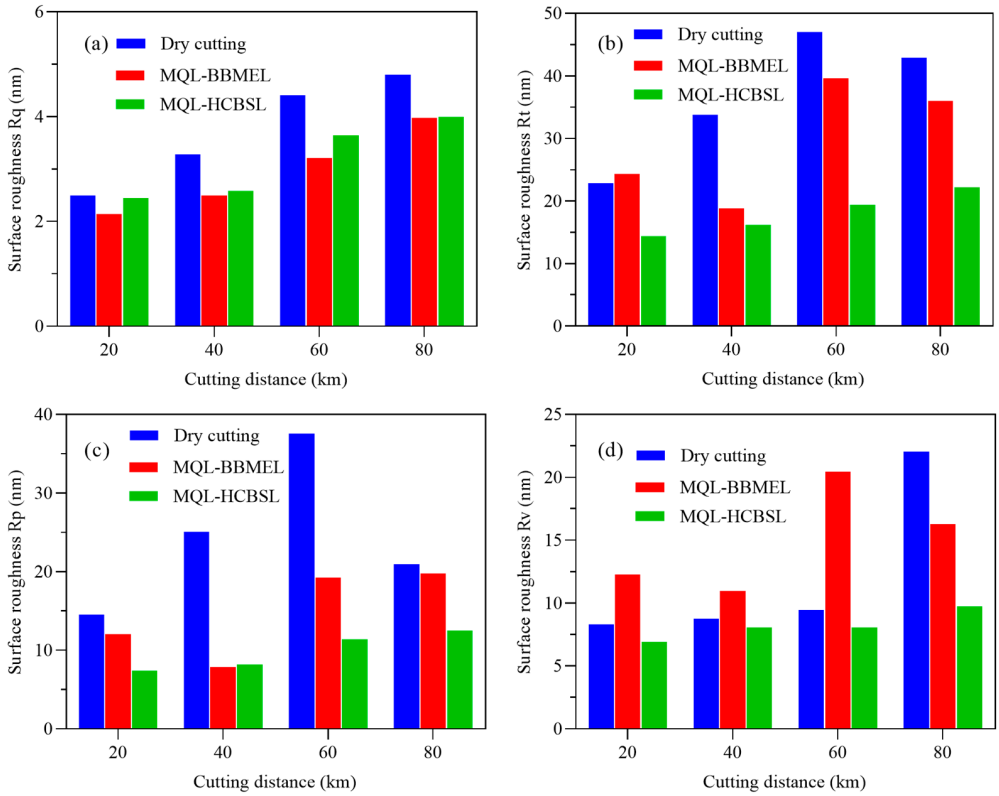



**Figure 4.** The variation of *Rq*, *Rt*, *Rp*, and *Rv* under dry cutting and MQL conditions at different cutting distances. (**a**) *Rq*; (**b**) *Rt*; (**c**) *Rp*; (**d**) *Rv*.

### 3.1.2. Surface Morphology of KDP Crystals Under Different Cutting Conditions

To investigate the factors influencing surface roughness variations, optical microscopy was employed to analyze the surface morphology of workpieces processed under different lubrication conditions. Figure 5 illustrates a comparison of surface morphology after 80 km of cutting under dry cutting and various lubrication conditions. As shown in Figure 5a, dry cutting resulted in the poorest surface quality, characterized by prominent scratches and large grooves aligned nearly parallel to the cutting direction. These grooves were primarily caused by tool wear and the relative motion between the tool and the workpiece, producing continuous and regular depressions on the surface. Scratches formed when detached chips from the adhered layer on the tool were dragged across the machined surface. Material accumulation occurred as these detached chips were compressed onto the workpiece surface, creating localized irregularities and point defects that further degraded the surface quality. In contrast, MQL-BBMEL produced the best surface quality. The grooves were narrow and shallow, with adhesion, material accumulation, and point defects nearly eliminated, as shown in Figure 5b. This improvement is attributed to the formation of a strong lubricating film, supported by the oil's superior heat dissipation properties. These properties effectively minimized adhesion and material deposition while also reducing tool wear. Furthermore, the lubricant's excellent flowability and spraying action efficiently removed chips from the cutting zone, preventing secondary damage to the surface. The oil also reduced adhesion between the tool and the workpiece surface, inhibiting chip buildup during the machining process and enhancing overall surface quality. Additionally, no fogging occurred on the crystal surface. However, MQL-HCBSL yielded slightly inferior results compared to MQL-BBMEL. The surface exhibited deeper and wider grooves, point defects, and the presence of liquid droplets, as shown in Figure 5c. This decline in performance is attributed to the higher viscosity of MQL-HCBSL, which reduced its fluidity and impaired atomization. As a result, the lubricant's penetration into the

cutting zone was less effective, leading to residual grooves and larger droplets that failed to form a uniform mist, ultimately compromising lubrication efficiency.

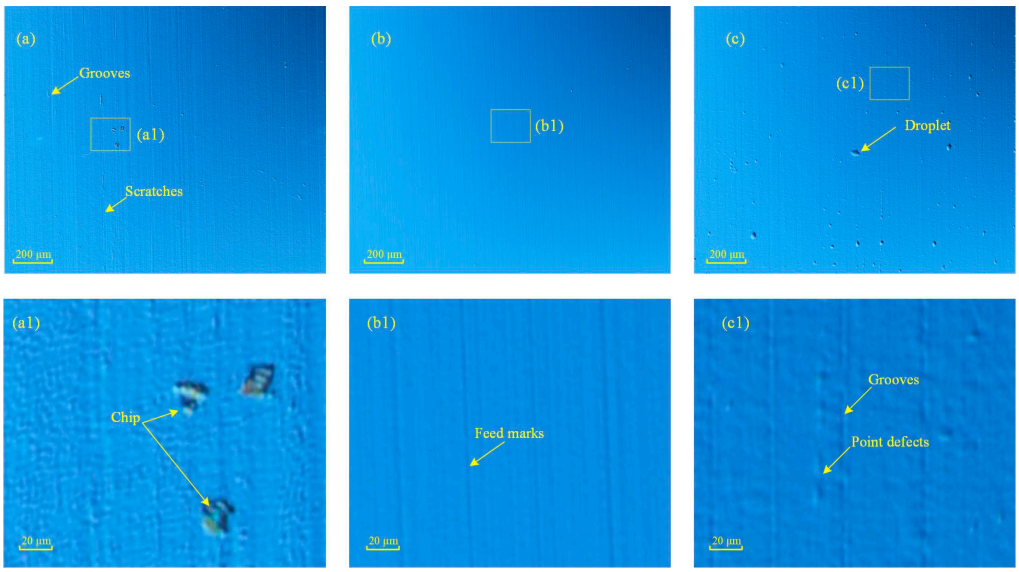



**Figure 5.** Surface morphology under dry cutting and MQL conditions after a cutting distance of 80 km. (**a**,**a1**) Dry cutting; (**b**,**b1**) MQL-BBMEL; (**c**,**c1**) MQL-HCBSL.

### *3.2. Tool Wear and Adhesion Mechanisms*

#### 3.2.1. Evolution of Tool Wear Under Dry Cutting and MQL Conditions

Diamond tools are extensively utilized in ultra-precision machining due to their sharp cutting edges [40,41]. In this study, the tool cutting edge radius was employed as a key metric to assess tool wear and cutting performance under different lubrication conditions during the initial wear stages. Figures 6 and 7 present tool cutting edge wear across various conditions. Dry cutting resulted in the most severe wear. Under MQL-BBMEL, the reduction in tool cutting edge radius wear was 21.28%, 28.41%, 20.59%, and 32.35% after the cutting distances of 20 km, 40 km, 60 km, and 80 km, respectively, with an average reduction of 25.16%. In comparison, MQL-HCBSL achieved reductions of 10.64%, 17.05%, 15.69%, and 15.44% over the same distances, resulting in an average reduction of 14.71%. Among the tested lubricants, MQL-BBMEL demonstrated the most substantial reduction in cutting edge wear. This superior performance is attributed to its ability to form a stable and uniform lubricating film at the tool–workpiece interface. This film effectively reduces friction and cutting forces, thereby significantly mitigating tool wear and extending tool life.

#### 3.2.2. Adhesion Layer Formation and Elemental Distribution on Tool Surfaces Under Dry Cutting and MQL Conditions

The studies described in this section, Section 3.2.2, were conducted prior to Section 3.2.1, with a primary focus on adhesion layer formation on tool surfaces under dry cutting and MQL conditions. Figure 8 presents SEM and EDS images of adhesive layers after a cutting distance of 80 km under different lubrication conditions. Under dry cutting, severe and non-uniform adhesion layers were evident (Figure 8a). The absence of lubrication resulted in direct tool–workpiece contact, amplifying friction and adhesion. This phenomenon was further intensified as oxygen-containing functional groups on the worn tool surface chemically bonded with chips, leading to the formation of adhesive layers [9]. EDS analysis (Figure 8d) verified that the adhered material was predominantly composed of workpiece chips, which exacerbated surface scratches and markedly deteriorated surface quality. In contrast, when using MQL-BBMEL, adhesion layers were effectively prevented, leaving

only a thin lubricating film on the tool surface (Figure 8b). This improvement is attributed to the polar functional groups in BBMEL, which facilitated the formation of a stable lubricating film through chemical or physical adsorption. The EDS analysis in Figure 8e shows only diamond components, confirming the absence of adhered chips and demonstrating the effectiveness of MQL-BBMEL in minimizing direct contact between the tool and workpiece. This suppression of adhesion significantly enhanced surface quality. However, under MQL-HCBSL, increased adhesion layers were observed (Figure 8c). This is due to HCBSL's higher viscosity, which caused large droplets to form on the tool surface, resembling flood lubrication rather than MQL. Additionally, the hydroxyl (-OH) groups in HCBSL, a partially ethoxylated trimethylene derivative ($C_3H_6(OCH_2CH_3)OH$), played a dual role. While they formed hydrogen bonds with the diamond tool surface, creating a lubricating film, they also interacted with hydrogen bonds in KDP chips, promoting chip adhesion. The EDS analysis in Figure 8f confirms the presence of adhered chips on the rake face, which significantly contributes to the degradation of surface quality.

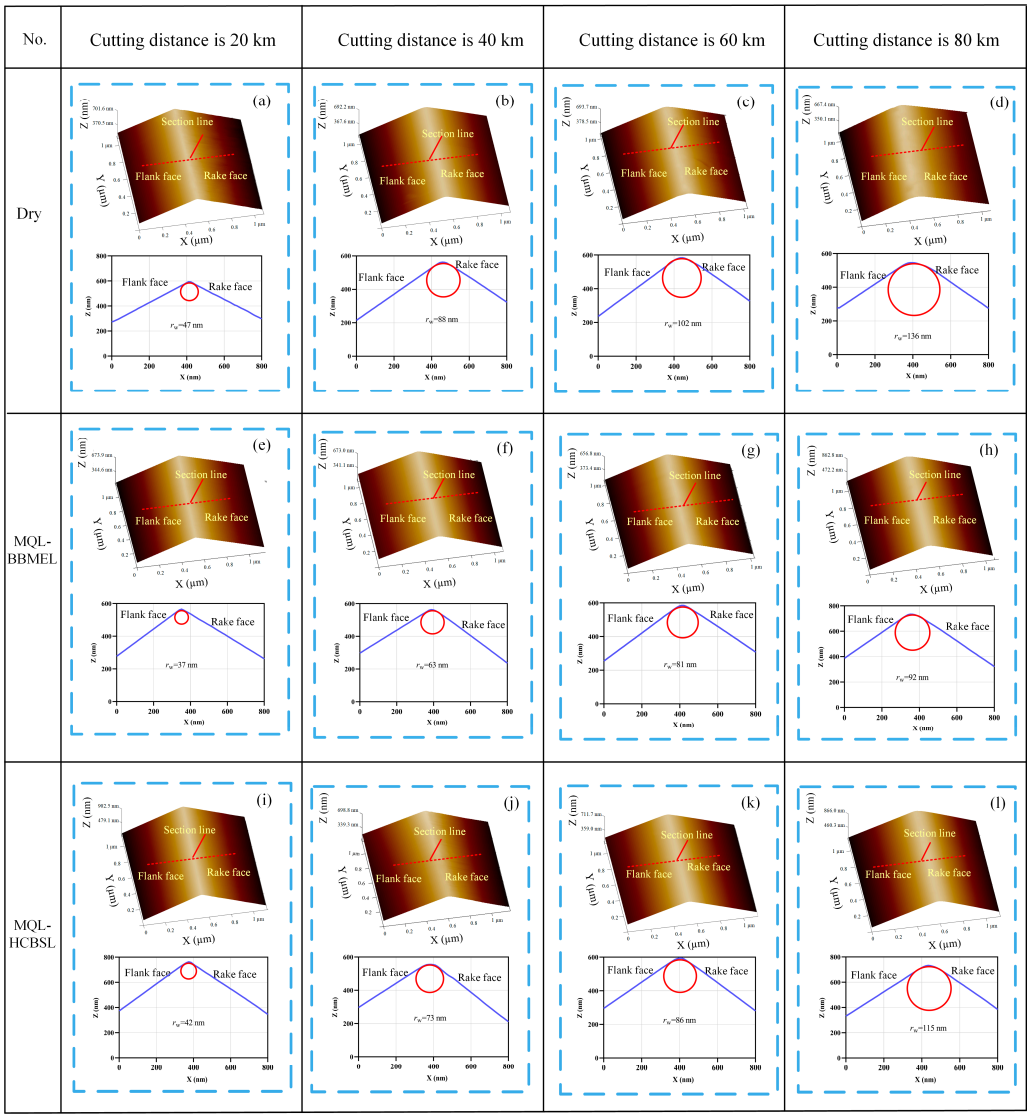



**Figure 6.** Tool cutting edge wear under dry cutting and MQL conditions at different cutting distances. (**a**) 20 km under dry cutting; (**b**) 40 km under dry cutting; (**c**) 60 km under dry cutting; (**d**) 80 km under dry cutting; (**e**) 20 km under MQL-BBMEL; (**f**) 40 km under MQL-BBMEL; (**g**) cutting distance of 60 km under MQL-BBMEL; (**h**) 80 km under MQL-BBMEL; (**i**) 20 km under MQL-HCBSL; (**j**) 40 km under MQL-HCBSL; (**k**) 60 km under MQL-HCBSL; (**l**) 80 km under MQL-HCBSL.

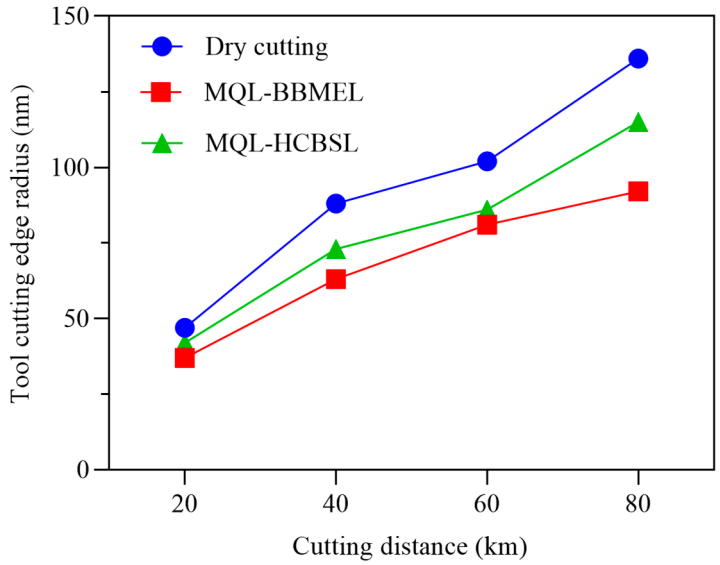



**Figure 7.** The variation of cutting edge radius under dry cutting and MQL conditions at different cutting distances.

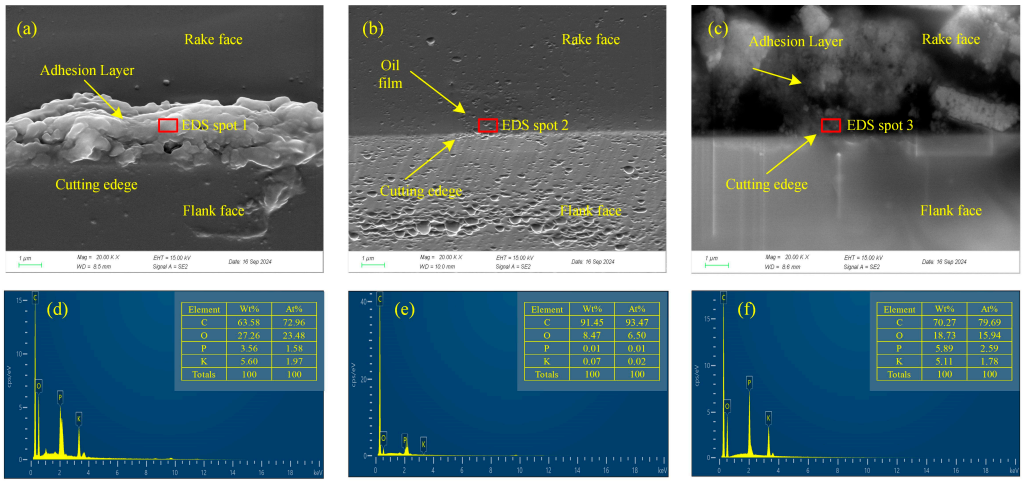



**Figure 8.** SEM and EDS images of adhesive layers on tool surfaces under dry cutting and MQL conditions after a cutting distance of 80 km. (**a**) SEM image of dry cutting; (**b**) SEM image of MQL-BBMEL; (**c**) SEM image of MQL-HCBSL. (**d**) EDS composition at Point 1 under dry cutting; (**e**) EDS composition at Point 2 under MQL-BBMEL; (**f**) EDS composition at Point 3 under MQL-HCBSL.

Figure 9 shows the elemental distribution on tool surfaces after a cutting distance of 80 km under different lubrication conditions. Under dry cutting, the sparse distribution of carbon (C) on the rake face and cutting edge indicates partial coverage by adhered chips. In contrast, elements such as oxygen (O), phosphorus (P), and potassium (K), characteristic of the workpiece material, are densely distributed, suggesting significant chip adhesion. When using MQL-BBMEL, the distribution of C and O is more uniform, while P and K are sparse, indicating that BBMEL forms a stable lubricating film that effectively prevents chip adhesion and improves surface integrity. However, under MQL-HCBSL, the denser distribution of O, P, and K compared to MQL-BBMEL suggests that HCBSL promotes chip adhesion due to its chemical composition, which enhances interactions between KDP chips and the worn tool surface. This observation definitively demonstrates that HCBSL is no longer a viable auxiliary lubricant for KDP crystal processing.

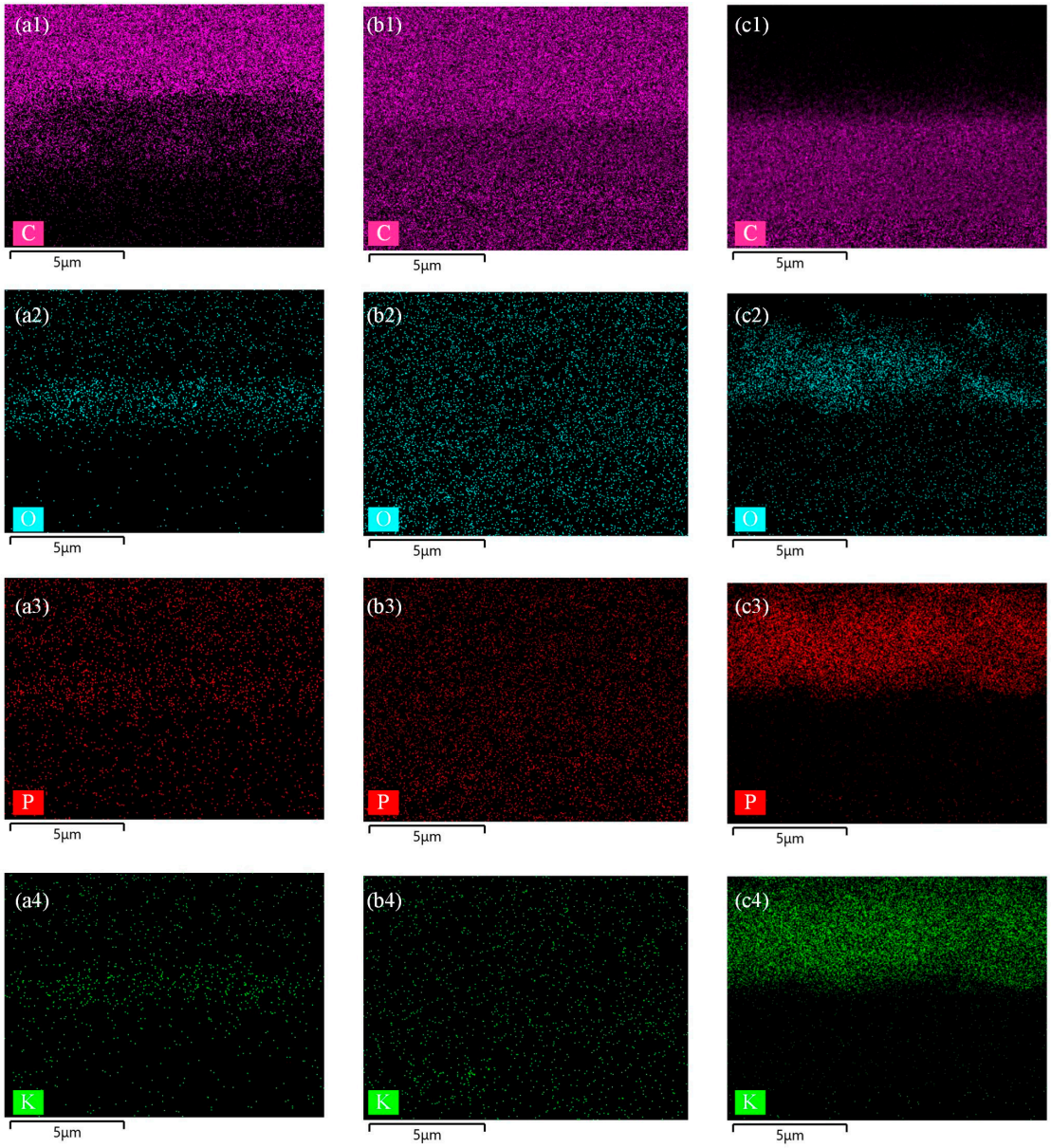



**Figure 9.** Element distribution of tool surfaces under dry cutting and MQL conditions after a cutting distance of 80 km. (**a1**–**a4**) Dry cutting; (**b1**–**b4**) MQL-BBMEL; (**c1**–**c4**) MQL-HCBSL.

### *3.3. Lubricating Film Formation and Composition Analysis*

#### 3.3.1. FTIR Spectroscopy of Functional Groups in BBMEL

To elucidate the formation mechanism of a stable lubricating film by BBMEL on the worn diamond tool surface, FTIR analysis was employed. However, detecting functional groups on the diamond surface using FTIR was not feasible because the oil film was too thin to be detected, and its uneven distribution further compromised the accuracy of reflectance or transmission signals. As a result, the properties of BBMEL were analyzed indirectly to investigate the formation and characteristics of the lubricating film. Figure 10a shows the FTIR spectrum of BBMEL. In the 3000–2800 $cm^{-1}$ range, the peak at 2959.4 $cm^{-1}$ is typically associated with the asymmetric C-H stretching vibration of methyl groups (-$CH_3$). Peaks at 2863.8 $cm^{-1}$ and 2924.6 $cm^{-1}$ correspond to the symmetric and asymmetric C-H stretching vibrations of saturated fatty acids (R-$CH_2$-R), indicating the presence of long-chain fatty acids that enhance lubrication. The peak at 1733.3 $cm^{-1}$ is attributed to the C=O stretching vibration of ester compounds (R-COO-R′). The strong polarity of the

carbonyl group (C=O) facilitates chemical adsorption onto the diamond surface, forming a stable oil film. Peaks at 1460.9 $cm^{-1}$ and 1382.6 $cm^{-1}$ correspond to $CH_2$ and $CH_3$ bending vibrations, further confirming the role of long-chain fatty acids in lubrication. Additionally, peaks at 1139.1 $cm^{-1}$ and 1168.1 $cm^{-1}$ correspond to ester bond vibrations (C=O and C-O), which enhance adsorption and improve the chemical stability of the lubrication film. The peak at 771 $cm^{-1}$ is associated with out-of-plane bending vibrations of C-H in alkyl chains (R-$CH_2$-R), contributing to the molecular stability of the oil. In conclusion, the oil's composition includes carbonyl (C=O), ester (R-COO-R′), and long-chain alkyl (R-$CH_2$-R) groups, which are present in the oil film formed on the diamond surface. While these functional groups may contribute to lubrication and tool protection through physical and chemical adsorption mechanisms, their specific roles as determining factors require further validation and analysis.

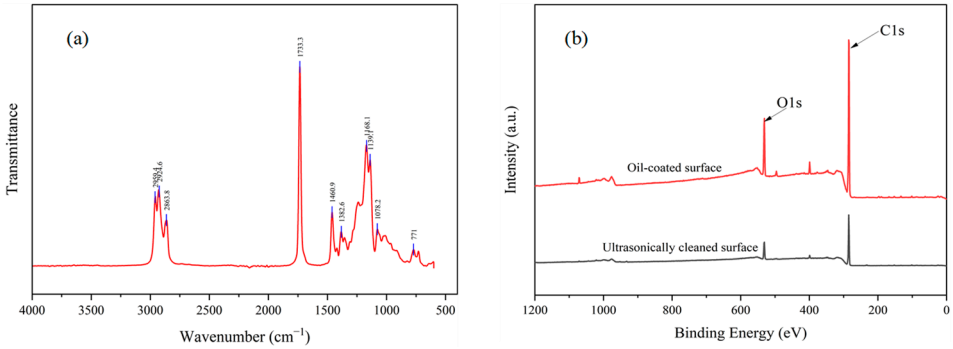



**Figure 10.** Chemical characterization of BBMEL and tool surface. (**a**) FTIR spectrum of BBMEL; (**b**) XPS survey spectra comparing the diamond tool surface with MQL-BBMEL oil film and after ultrasonic cleaning (cutting distance: 80 km).

### 3.3.2. XPS Analysis of Lubricant Adsorption on Worn Tool Surfaces with BBMEL

To further investigate the nature of oil film formation on worn tool surfaces, XPS analysis was performed on diamond surfaces both coated with oil and ultrasonically cleaned. As shown in Figure 10b the oil-coated surface exhibited distinct C1s and O1s peaks, indicating the adsorption of oxygen-containing functional groups from BBMEL. In contrast, the ultrasonically cleaned surface displayed a marked reduction in oxygen-related signals, dominated by C-C ($sp^3$) bonds characteristic of the diamond's intrinsic structure.

To further investigate the functional groups responsible for the adsorption of the oil film on the diamond surface, high-resolution XPS spectra were analyzed, as shown in Figure 11. As seen in Figure 11a, the detailed C1s spectrum of the oil-coated diamond surface reveals a dominant peak at 284.88 eV, corresponding to C–C ($sp^3$) bonds, which reflect the diamond's intrinsic structure or saturated carbon chains in the oil (e.g., long-chain alkanes or saturated fatty acids). A smaller peak at 284.08 eV is attributed to C–C ($sp^2$) bonds, indicating the presence of unsaturated carbon chains or C=C double bonds, such as those found in unsaturated fatty acid components. Peaks at 283.58 eV and 282.88 eV suggest the presence of hydrocarbon chains or long-chain saturated fatty acids from BBMEL. Additionally, the peak at 286.28 eV corresponds to C–O bonds, associated with ester or hydroxyl groups, while the 287.28 eV peak indicates C=O bonds from carbonyl groups. These findings confirm the presence of polar functional groups with a strong adsorption potential on the diamond surface. The O1s spectrum, shown in Figure 11b, further validates these functional groups. The peak at 532.98 eV corresponds to C–O–C (ether groups), while the 532.08 eV peak is attributed to C=O bonds in ester groups (R–COO–R′). The 531.38 eV peak corresponds to C=O bonds from carbonyl groups, likely derived from the unsaturated fatty acids in the oil. Additionally, the 530.58 eV peak suggests the presence of C–O bonds

in surface oxides, possibly formed through chemical interactions between BBMEL and the diamond surface during cutting.

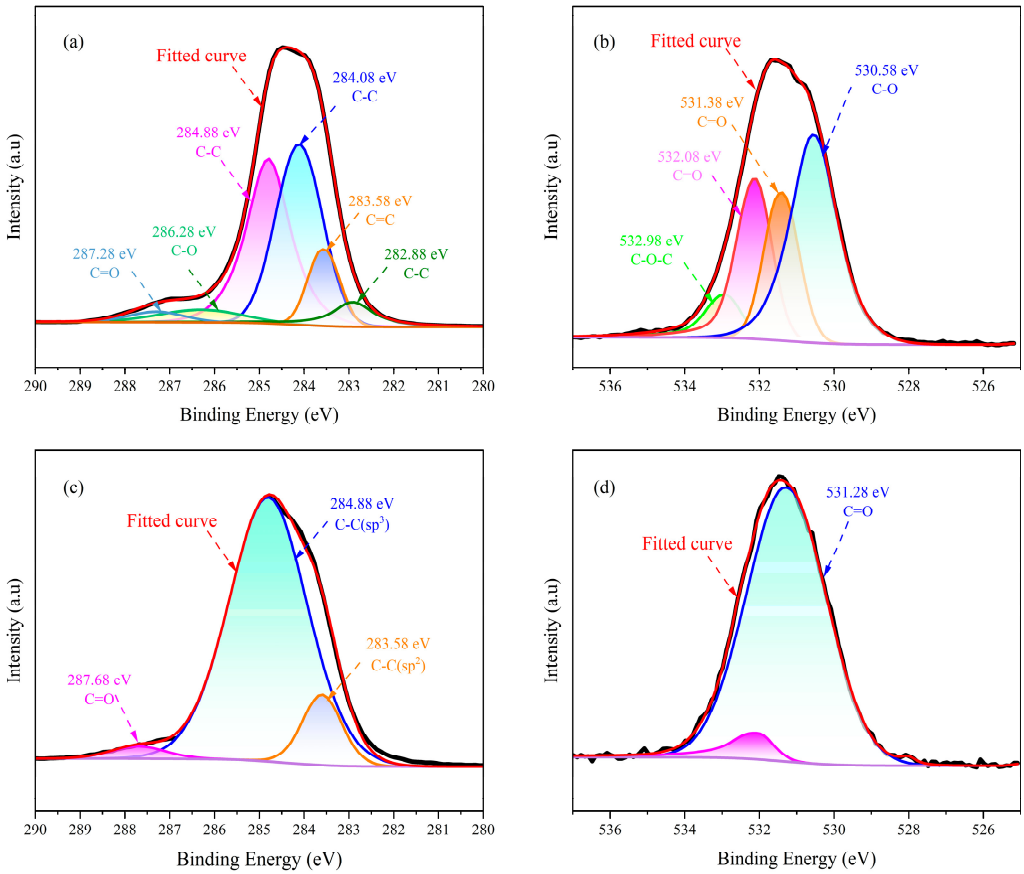



**Figure 11.** XPS spectra of diamond tool surfaces with a lubrication film and after ultrasonic cleaning. (**a**) C1s spectrum with lubrication film; (**b**) O1s spectrum with lubrication film; (**c**) C1s spectrum after ultrasonic cleaning; (**d**) O1s spectrum after ultrasonic cleaning.

After ultrasonic cleaning, the dominant C1s peak at 284.88 eV (C–C $sp^3$), as shown in Figure 11c, indicates that most extraneous compounds have been removed, revealing the underlying diamond structure. However, as seen in Figure 11d, the persistence of minor peaks at 283.58 eV (C–C $sp^2$) and 286.28 eV (C–O), along with residual O1s signals, suggests that certain oxygen-containing functional groups remain adsorbed. These polar groups, originating from the unsaturated fatty acids in the oil, appear to chemically bond with the worn diamond surface. In other words, the presence of C–O and related oxygen-rich sites facilitate the stable chemical adsorption of the oil film.

### 3.3.3. Mechanism of Lubricating Film Formation in MQL Cutting

The mechanism behind the formation of lubricating films in the cutting zone was analyzed, as detailed in Sections 3.3.1–3.3.3. Under MQL-BBMEL conditions, the interaction between the KDP crystal and the lubricant was thoroughly examined to provide a systematic understanding of the process. Figure 12 illustrates the mechanism of the lubricating film formation mechanism in MQL-BBMEL cuttings. For new diamond tools, the surface is predominantly terminated with hydrogen (C-H), resulting in a chemically stable and inert surface. In this case, mixed fat molecules adhere through physical adsorption, forming a stable, physical adsorption film. This film helps reduce friction but is primarily governed by weaker physical interactions. For worn diamond tools, the surface undergoes significant transformations as the fly-cutting process progresses. Mechanical stress induces surface

amorphization [42], leading to the formation of oxygen-containing functional groups [9]. During MQL-BBMEL-assisted fly-cutting, functional groups in BBMEL, such as hydroxyl (-OH), carbonyl (C=O), ester (R-COO-R′), and long-chain alkyl chains (R-$CH_2$-R′), interact with the oxygen-containing tool surface, increasing its chemical reactivity. This facilitates strong chemical adsorption of polar molecules from the mixed-fat lubricant, contributing to improved lubrication performance. This chemical interaction forms a robust boundary lubricating film, offering enhanced stability and wear resistance. The lubricating film, particularly on worn tools, remains intact during cutting due to the mixed fat's high viscosity and chemical stability. It effectively isolates chips from the tool surface, preventing adhesion layer formation that can compromise surface quality. Moreover, the excellent heat dissipation properties of mixed fat help lower the friction coefficient and cutting zone temperature, further enhancing the quality of the machined surface. This dual interaction mechanism demonstrates the adaptability and superior performance of mixed-fat-based lubricants in ultra-precision machining.

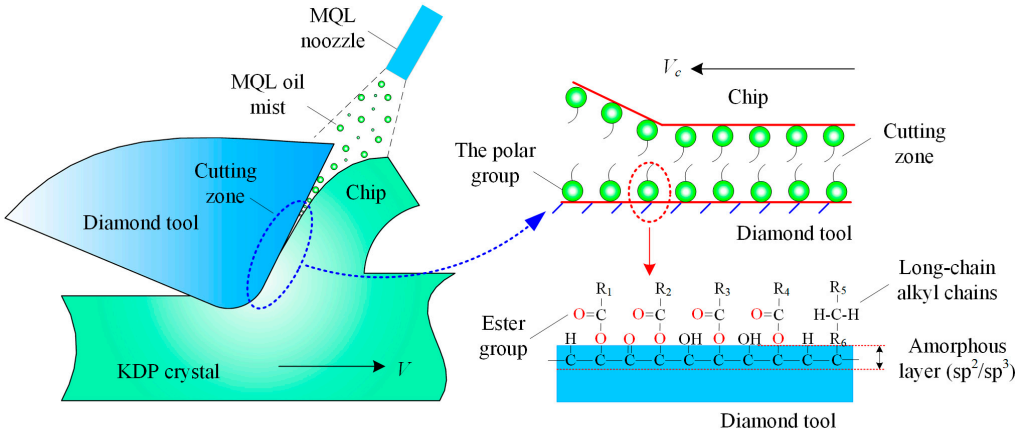



**Figure 12.** Schematic illustration of the lubricating film formation mechanism in MQL-BBMEL cutting.

### *3.4. Effect of BBMEL on the Surface Integrity of KDP Crystals*

To evaluate whether BBMEL induces deliquescence, fogging, or chemical reactions on KDP crystal surfaces, the lubricant was first removed using toluene. The cleaned crystal surfaces and subsurfaces were then analyzed using GIXRD and Raman spectroscopy, as shown in Figure 13. The results were compared with those obtained from bulk material KDP crystals to assess potential structural and chemical changes.

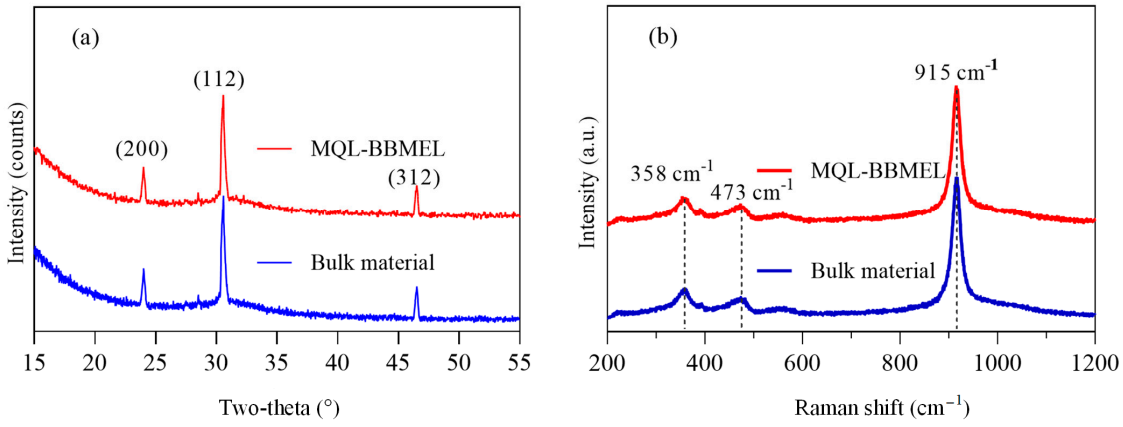



**Figure 13.** GIXRD and Raman spectra of KDP crystals under MQL-BBMEL after a cutting distance of 80 km. (**a**) GIXRD spectra; (**b**) Raman spectra.

As shown in Figure 13a, GIXRD analysis detected multiple diffraction peaks in the subsurface of KDP crystals processed under MQL-BBMEL conditions, including (200), (112), and (312). These peaks, highlighted by the red line, confirm that the crystal structure remains unchanged compared to bulk material KDP, indicating that MQL-BBMEL-assisted cutting does not induce subsurface damage. Furthermore, optical micrographs, as shown in Figure 13b, revealed no signs of deliquescence, reinforcing the effectiveness of BBMEL in preserving the crystal's structural integrity. To further assess the impact of BBMEL on the processed surface, Raman spectroscopy was performed after surface cleaning, as shown in Figure 10b. The Raman spectra from dry cutting and MQL cutting with BBMEL exhibited no significant differences from the original KDP surface, confirming the absence of chemical alterations. This stability is attributed to the lubricant's extremely low water content and its composition of saturated fatty acids and lipids, which lack reactive groups capable of interacting with KDP.

## 4. Conclusions

This study examined the lubrication performance and mechanisms of mixed-fat, oil-based MQL in the ultra-precision fly-cutting of KDP crystals, with a focus on surface roughness, tool wear, and surface integrity. The findings confirm that MQL-BBMEL consistently outperforms MQL-HCBSL, leading to improved machining performance:

(1) MQL-BBMEL exhibited significantly better performance than MQL-HCBSL in enhancing surface quality when compared to dry cutting, achieving reductions of 27.77% in *Sa* and 44.76% in *Sq*. In contrast, MQL-HCBSL showed reductions of 16.94% in *Sa* and 27.55% in *Sq* under the same conditions. This superior efficacy of MQL-BBMEL in minimizing surface defects, such as scratches and grooves, is attributed to the formation of stable lubricating films facilitated by polar functional groups. These films effectively reduced groove formation, adhesion, and point defects, while also improving heat dissipation and chip removal efficiency.

(2) MQL-BBMEL exhibited notably superior performance in minimizing tool wear, achieving a 25.16% reduction compared to dry cutting, which significantly surpassed the 14.71% reduction attained by MQL-HCBSL. This improvement is primarily due to MQL-BBMEL's lower viscosity and active functional groups (-OH, R-$CH_2$-R′, and R-COO-R′), which enhance atomization and penetration into the cutting zone. These characteristics promote the formation of robust and uniform lubricating films, effectively minimizing adhesion, reducing friction, and improving wear resistance, especially in worn tools.

(3) GIXRD and Raman spectroscopy confirm that MQL-BBMEL prevents KDP deliquescence, surface fogging, and impurity adsorption. This stability stems from the lubricant's minimal water content and composition of saturated fatty acids and lipids, which lack reactive groups for KDP interaction.

Despite these promising results, certain limitations remain. The long-term stability and scalability of the lubricating film under dynamic machining conditions require further investigation. Future research should focus on optimizing mixed fat formulations, incorporating functional nanoparticle additives, and evaluating performance under high-speed and high-load machining conditions. Additionally, exploring its applicability to other brittle materials such as glass and silicon could further expand its industrial relevance. These findings establish mixed-fat-based MQL as a sustainable and efficient lubrication strategy, contributing to green manufacturing practices while advancing precision machining of brittle materials.

**Author Contributions:** X.Y.: methodology, software, conceptualization and writing—original draft; F.Z.: funding acquisition and supervision; S.Z. and J.Z.: data curation and investigation; D.L.: formal analysis and validation; X.L. and J.W.: validation; J.D.: reviewing and editing. All authors have read and agreed to the published version of the manuscript.

**Funding:** This research was funded by the National Natural Science Foundation of China (Grant No. 51975154) and The Natural Science Foundation of Sichuan Province, China (Grant No. 2024NSFSC0148).

**Data Availability Statement:** The data presented in this study are available on request from the corresponding author. The data are not publicly available due to restrictions of privacy.

**Acknowledgments:** We sincerely thank the reviewers and editors for their insightful and constructive feedback, which has greatly improved the quality of this paper.

**Conflicts of Interest:** The authors declare no conflict of interest.

## References

1. Deng, L.; Yang, H.; Zeng, X.; Wu, B.; Liu, P.; Wang, X.; Duan, J. Study on mechanics and key technologies of laser nondestructive mirror-separation for KDP crystal. *Int. J. Mach. Tools Manuf.* **2015**, *94*, 26–36. [CrossRef]
2. Li, C.; Zhang, Y.; Zhou, G.; Wei, Z.; Zhang, L. Theoretical modelling of brittle-to-ductile transition load of KDP crystals on (001) plane during nanoindentation and nanoscratch tests. *J. Mater. Res. Technol.* **2020**, *9*, 14142–14157. [CrossRef]
3. Nakamoto, T.; Takahashi, C.; Furukawa, T. Polishing of Potassium Dihydrogen Phosphate Single Crystal in Saturated Solution by Laser Beam Scanning:—Polishing Conditions and Surface Roughness&mdash. *J. Jpn. Soc. Precis. Eng.* **2015**, *81*, 763–767. [CrossRef]
4. Ji, F.; Xu, M.; Wang, B.; Wang, C.; Li, X.; Zhang, Y.; Zhou, M.; Huang, W.; Wei, Q.; Tang, G.; et al. Preparation of methoxyl poly(ethylene glycol) (MPEG)-coated carbonyl iron particles (CIPs) and their application in potassium dihydrogen phosphate (KDP) magnetorheological finishing (MRF). *Appl. Surf. Sci.* **2015**, *353*, 723–727. [CrossRef]
5. Namba, Y.; Katagiri, M. Ultraprecision grinding of potassium dihydrogen phoshate crystals for getting optical surfaces. In *Laser-Induced Damage in Optical Materials: 1998*; Exarhos, G.J., Guenther, A.H., Kozlowski, M.R., Lewis, K.L., Soileau, M.J., Eds.; SPIE: Bellingham, WA, USA, 1999; Volume 3578, pp. 692–693. [CrossRef]
6. Hou, N.; Zhang, L.C.; Zhang, Y.; Zhang, F.H. On the Ultra-Precision Fabrication of Damage-Free Optical KDP Components: Mechanisms and Problems. *Crit. Rev. Solid State Mat. Sci.* **2019**, *44*, 283–297. [CrossRef]
7. Li, C.; Piao, Y.; Hu, Y.X.; Wei, Z.Z.; Li, L.Q.; Zhang, F.H. Modelling and experimental investigation of temperature field during fly-cutting of KDP crystals. *Int. J. Mech. Sci.* **2021**, *210*, 106751. [CrossRef]
8. An, C.H.; Feng, K.; Wang, W.; Xu, Q.; Lei, X.Y.; Zhang, J.F.; Yao, X.L.; Li, H.B. Interaction Mechanism of Thermal and Mechanical Field in KDP Fly-Cutting Process. *Micromachines* **2021**, *12*, 855. [CrossRef]
9. Yao, X.; Zhang, F.; Zhang, J.; Zhang, S.; Liao, D.; Lei, X.; Wang, J. Transient Stress-Induced Tool Wear Mechanisms and Adhesive Layer Formation in Single-Point Diamond Fly-Cutting of KDP Crystals. *Mater. Today Commun.* **2025**, *43*, 111648. [CrossRef]
10. Hu, L.; Wang, Z.; Wang, J.; Wang, Y. Derivative analysis and evaluation of roll-slip fretting wear mechanism of ultra-thin-walled bearings under high service. *Wear* **2025**, *562*, 205630. [CrossRef]
11. Hu, L.; Li, B.; Wang, Z.; Wang, Y. Analysis and evaluation of multi-state wear mechanism of elastic-flexible thin-walled bearings. *Tribol. Int.* **2025**, *202*, 110293.
12. Hu, L.; Pueh, L.H.; Wang, Z.; Wang, Y. Surface Performance Control and Evaluation of Precision Bearing Raceway with Wireless Sensing CBN Grinding Wheel. *Wear* **2025**, *568*, 205966.
13. Lai, H.; Pengyang, J.; Zixi, W.; Yuming, W. Study on type of magnetic suspension rotor groove and wear of drop touchdown bearing. *Eng. Appl. Comput. Fluid. Mech.* **2024**, *18*, 2422065.
14. Fuchs, B.A.; Hed, P.P.; Baker, P.C. Fine diamond turning of KDP Crystals. *Appl. Opt.* **1986**, *25*, 1733–1735. [CrossRef]
15. Kozlowski, M.R.; Thomas, I.M.; Edwards, G.J.; Stanion, K.A.; Latanich, L. Influence of diamond turning and surface cleaning processes on the degradation of KDP crystal surfaces. *Proc. SPIE* **1991**, *1561*, 59–69.
16. Lawal, S.A.; Choudhury, I.A.; Nukman, Y. A critical assessment of lubrication techniques in machining processes: A case for minimum quantity lubrication using vegetable oil-based lubricant. *J. Clean. Prod.* **2013**, *41*, 210–221. [CrossRef]
17. Li, G.X.; Chandra, S.; Rashid, R.; Palanisamy, S.; Ding, S.L. Machinability of additively manufactured titanium alloys: A comprehensive review. *J. Manuf. Process.* **2022**, *75*, 72–99. [CrossRef]
18. Sílvia, R.C.; Lauro, C.H.; Ana, H.; Davim, J.P. Development of FEM-based digital twins for machining difficult-to-cut materials: A roadmap for sustainability. *J. Manuf. Process.* **2022**, *75*, 739–766. [CrossRef]

19. Wang, Y.; Liu, C.F. State-of-the-art on minimum quantity lubrication in green machining. *J. Clean. Prod.* **2023**, *429*, 139613. [CrossRef]
20. Saha, S.; Deb, S.; Bandyopadhyay, P.P. Shadow zone in MQL application and its influence on lubricant deficiency and machinability during micro-milling. *Int. J. Mech. Sci.* **2022**, *220*, 107181. [CrossRef]
21. Saha, S.; Deb, S.; Bandyopadhyay, P.P. Progressive wear based tool failure analysis during dry and MQL assisted sustainable micro-milling. *Int. J. Mech. Sci.* **2021**, *212*, 106844. [CrossRef]
22. Saha, S.; Deb, S.; Bandyopadhyay, P.P. An analytical approach to assess the variation of lubricant supply to the cutting tool during MQL assisted high speed micromilling. *J. Mater. Process. Technol.* **2020**, *285*, 116783. [CrossRef]
23. Sayuti, M.; Erh, O.M.; Sarhan, A.A.; Hamdi, M. Investigation on the morphology of the machined surface in end milling of aerospace AL6061-T6 for novel uses of SiO2 nanolubrication system. *J. Clean. Prod.* **2014**, *66*, 655–663. [CrossRef]
24. Zhou, X.; He, L.; Yuan, S.; Deng, J.; Su, Z.; Yang, J.; Du, F. Experimental Research on the Effect of Thermophysical Characteristics of Cutting Fluid on Cutting Performance During Turning Ti-6Al-4V Alloy. *Lubricants* **2025**, *13*, 90. [CrossRef]
25. Su, Y.; Gong, L.; Li, B.; Liu, Z.; Chen, D. Performance evaluation of nanofluid MQL with vegetable-based oil and ester oil as base fluids in turning. *Int. J. Adv. Manuf. Technol.* **2016**, *83*, 2083–2089. [CrossRef]
26. Li, L.; Xu, J.; Guo, G.; Gupta, M.K.; Chen, M. Wear behavior of different coated tools in MQL-assisted milling of magnesium-based rare-earth alloys. *J. Mater. Res. Technol.* **2023**, *27*, 1665–1682. [CrossRef]
27. Guo, S.; Li, C.; Zhang, Y.; Wang, Y.; Li, B.; Yang, M.; Zhang, X.; Liu, G. Experimental evaluation of the lubrication performance of mixtures of castor oil with other vegetable oils in MQL grinding of nickel-based alloy. *J. Clean. Prod.* **2017**, *140*, 1060–1076. [CrossRef]
28. Xu, W.; Li, C.; Zhang, Y.; Ali, H.M.; Sharma, S.; Li, R.; Yang, M.; Gao, T.; Liu, M.; Wang, X.; et al. Electrostatic atomization minimum quantity lubrication machining: From mechanism to application. *Int. J. Extreme Manuf.* **2022**, *4*, 42003. [CrossRef]
29. Luo, X.C.; Wu, S.J.; Wang, D.Z.; Yun, Y.X.; An, Q.L.; Li, C.H. Sustainable development of cutting fluids: The comprehensive review of vegetable oil. *J. Clean. Prod.* **2024**, *473*, 143544. [CrossRef]
30. Uslu, G.; Korkmaz, M.E.; Elkilani, R.H.R.; Gupta, M.K.; Vashishtha, G. Investigation of tribological properties of inconel 601 under environmentally friendly MQL and Nano-Fluid MQL with pack boronizing. *Lubricants* **2024**, *12*, 353. [CrossRef]
31. Kara, F. Investigation of the effect of Al2O3 nanoparticle-added MQL lubricant on sustainable and clean manufacturing. *Lubricants* **2024**, *12*, 393. [CrossRef]
32. Zhang, X.; Li, C.; Zhou, Z.; Liu, B.; Zhang, Y.; Yang, M.; Gao, T.; Liu, M.; Zhang, N.; Said, Z.; et al. Vegetable Oil-Based Nanolubricants in Machining: From Physicochemical Properties to Application. *Chin. J. Mech. Eng.* **2023**, *36*, 76. [CrossRef]
33. Debnath, S.; Anwar, M.; Pramanik, A.; Basak, A.K. Nanofluid-minimum quantity lubrication system in machining: Towards clean manufacturing. In *Sustainable Manufacturing*; Elsevier: Amsterdam, The Netherlands, 2021; pp. 109–135. [CrossRef]
34. Lisowicz, J.; Habrat, W.; Krupa, K. Influence of minimum quantity lubrication using vegetable-based cutting fluids on surface topography and cutting forces in finish turning of Ti-6Al-4V. *Adv. Sci. Technol. Res. J.* **2022**, *16*. [CrossRef]
35. Farfan-Cabrera, L.I.; Rojo-Valerio, A.; Calderon-Najera, J.D.D.; Coronado-Apodaca, K.G.; Iqbal, H.M.; Parra-Saldivar, R.; Franco-Morgado, M.; Elias-Zuñiga, A. Microalgae oil-based metal working fluids for sustainable minimum quantity lubrication (MQL) operations—A perspective. *Lubricants* **2023**, *11*, 215. [CrossRef]
36. Panda, D.; Kumari, K.; Dalai, N. Performance of Minimum Quantity Lubrication (MQL) and its effect on Dry Machining with the addition of Nano-particle with the biodegradable base fluids: A review. *Mater. Today-Proc.* **2022**, *56*, 1298–1301. [CrossRef]
37. Zbek, N.A.; Zbek, O.; Kara, F.; Saruhan, H. Effect of Eco-Friendly Minimum Quantity Lubrication in Hard Machining of Vanadis 10: A High Strength Steel. *Steel Res. Int.* **2022**, *93*, 19.
38. dos Santos Motta Neto, W.; Leal, J.E.; Arantes, L.J.; Arencibia, R.V. The effect of stylus tip radius on Ra, Rq, Rp, Rv, and Rt parameters in turned and milled samples. *Int. J. Adv. Manuf. Technol.* **2018**, *99*, 1979–1992.
39. Dobes, J.; Leal, J.E.S.; Profeta, J.; de Sousa, M.M.; Neto, F.P.L.; Piratelli-Filho, A.; Arencibia, R.V. Effect of mechanical vibration on Ra, Rq, Rz, and Rt roughness parameters. *Int. J. Adv. Manuf. Technol.* **2017**, *92*, 393–406.
40. Cui, Z.P.; Li, G.; Liu, H.Z.; Zong, W.J.; Zhang, H.J.; Zhang, C.Y.; Du, K. Tool anisotropic wear prediction and its influence on surface topography in diamond turning of oxygen-free copper. *J. Mater. Process. Technol.* **2023**, *318*, 118042. [CrossRef]
41. Du, J.B.; Liu, H.Z.; Yang, N.; Chen, X.Z.; Zong, W.J. Modification of diamond tool by focused ion beam in dry single-point diamond turning. *Appl. Surf. Sci.* **2023**, *637*, 157882. [CrossRef]
42. Yang, N.; Yang, X.; Huang, W.; Zhao, S.; Lei, D.J. Analysis of diamond tool wear mechanism in terms of stress for KDP Fly cutting. *Mater. Today Commun.* **2022**, *30*, 103146. [CrossRef]


**Disclaimer/Publisher's Note:** The statements, opinions and data contained in all publications are solely those of the individual author(s) and contributor(s) and not of MDPI and/or the editor(s). MDPI and/or the editor(s) disclaim responsibility for any injury to people or property resulting from any ideas, methods, instructions or products referred to in the content.